

RESEARCH

Open Access



Development of attenuated Orf virus as a safe oncolytic viral vector for nasopharyngeal carcinoma treatment

Yumiko Yamada¹, Yu-Chih Wang², Hao-Ping Liu³, Greg Ryan Gerongano⁴, Ching-Yu Tseng¹, Shu-Chen Liu⁵, Guan-Ru Liao¹, Chao-Chin Chang¹, Jiunn-Wang Liao², Mei-Lin Wang⁶, Yuan-Yen Chang⁶, Fong-Yuan Lin⁷ and Wei-Li Hsu^{1,8*}

Abstract

Background Orf virus (ORFV) is gaining attention as a promising viral vector for cancer therapy because of its unique properties. Recent studies have shown that ORFV could be effective against various cancers, particularly nasopharyngeal carcinoma. This research explores the ability of wild-type ORFV and recombinant ORFVs, which lack specific virulence factors, to kill NPC cells and modulate the immune response.

Methods Two NPC cell lines, HK1 (from Hong Kong) and TW02 (from Taiwan), were infected with wild-type ORFV and two recombinant ORFVs lacking either vascular endothelial growth factor (VEGF) or chemokine binding protein (CBP) virulence factors. The oncolytic effects were evaluated by assessing cell death pathways, particularly pyroptosis, which was monitored through the cleavage of gasdermin E (GSDME). The activation of survival pathways, such as focal adhesion kinase (FAK) and AKT, was also analyzed. In addition, the influence of ORFV infection on natural killer (NK) cell recruitment and cytotoxicity was investigated. In vivo experiments were conducted in a xenograft mouse model in which HK1 tumors were used to evaluate the antitumor activity of wild-type ORFV and two deletion-mutant ORFVs.

Results Wild-type ORFV effectively killed NPC cells, especially HK1 cells. The recombinant ORFVs, despite being attenuated by the loss of VEGF or CBP, retained the ability to infect and cause NPC cell death, with the CBP-deleted virus showing notable effectiveness in HK1 cells. Early ORFV infection led to pyroptosis via GSDME cleavage, causing cell detachment and a reduction in FAK and AKT activation. ORFV also enhanced NK cell recruitment and boosted NK cell-mediated cytotoxicity in infected NPC cells. In the HK1 xenograft model, CBP-deleted ORFV significantly inhibited tumor growth.

Conclusion ORFV, particularly the wild-type and CBP-deleted variants, has significant potential as an oncolytic viral vector for NPC therapy. It induces cell death via pyroptosis and enhances immune-mediated tumor cell destruction through NK cells. The attenuated CBP-deleted ORFV offers a safer and effective option for cancer treatment, making it a promising candidate for future therapeutic applications.

Keywords Oncolytic-attenuated ORFV, Nasopharyngeal carcinoma, NK cells, Cell death, Xenograft model

*Correspondence:

Wei-Li Hsu
wlhsu@dragon.nchu.edu.tw

Full list of author information is available at the end of the article



© The Author(s) 2025. **Open Access** This article is licensed under a Creative Commons Attribution-NonCommercial-NoDerivatives 4.0 International License, which permits any non-commercial use, sharing, distribution and reproduction in any medium or format, as long as you give appropriate credit to the original author(s) and the source, provide a link to the Creative Commons licence, and indicate if you modified the licensed material. You do not have permission under this licence to share adapted material derived from this article or parts of it. The images or other third party material in this article are included in the article's Creative Commons licence, unless indicated otherwise in a credit line to the material. If material is not included in the article's Creative Commons licence and your intended use is not permitted by statutory regulation or exceeds the permitted use, you will need to obtain permission directly from the copyright holder. To view a copy of this licence, visit <http://creativecommons.org/licenses/by-nc-nd/4.0/>.

Introduction

Developing countries are currently facing a significant challenge, as cancer has emerged as the leading cause of death, with the number of cases projected to rise annually [1]. Over the years, various strategies for successful cancer treatment, such as cell-based vaccines [2] and checkpoint inhibitors [3], have been developed. Despite these advances, the average response rate to new cancer treatments remains less than 15% [4]. In light of these limitations, biological therapies i.e., oncolytic virotherapy have emerged as promising alternatives alongside traditional treatments such as chemotherapy and radiotherapy.

Oncolytic viruses (OVs) selectively attack cancer cells while leaving healthy cells largely unaffected [5]. The primary mechanism of action involves self-amplification within tumor sites, enabling the infection of distant metastases and ultimately resulting in the direct destruction of cancer cells [6]. Additionally, OVs can mediate antitumor effects through mechanisms beyond direct cell lysis, such as disrupting the tumor vasculature and enhancing the immune response [7]. For example, vesicular stomatitis virus induces tumor inflammation, reducing blood flow and causing tumor cell death [8]. OVs leverage various biological pathways, including metabolism, proliferation, and cell death processes, to optimize their oncolytic activity and evade immune detection [9].

Several viruses, including herpesviruses, adenoviruses, influenza viruses, and poxviruses, have demonstrated oncolytic potential. Among these, poxviruses stand out for their ability to elicit long-lasting immune responses, particularly cytotoxic T lymphocytes (CTLs) and antibodies [10–12]. Poxviruses, which replicate exclusively in the cytoplasm, present minimal risk of integrating their genetic material into the host genome. This, combined with their large genome size and precise gene regulation, makes them suitable candidates for genetic engineering. These characteristics allow for the attenuation of poxviruses or the insertion of specific genes for therapeutic purposes [13]. Additionally, poxviruses can selectively infect tumor cells due to specific features of the tumor microenvironment. For example, the myxoma virus replicates in tumor cells with elevated phosphorylated AKT [14], and the vaccinia virus targets cells with activated EGFR-Ras signaling, which is common in many tumors [15]. Three strains of oncolytic vaccinia viruses, Wyeth (Pexa-Vec), Western Reserve (TG6002), and Lister (GL-ONC1), have undergone clinical trials [16]. Pexa-Vec, a genetically modified vaccinia virus expressing granulocyte-macrophage colony-stimulating factor (GM-CSF), has shown promise in treating hepatocellular carcinoma, improving patient tolerance and extending lifespan [17–19].

Orf virus (ORFV), a parapoxvirus that causes skin infections in goats and sheep, has demonstrated potential

as an oncolytic agent in various cancer models [20–25]. For example, ORFV infection resulted in tumor regression in murine models of human lung carcinoma (A549) [21]. Additionally, a closely related chimeric parapoxvirus, CF189, showed cytotoxic effects on triple-negative breast cancer cells and antitumor activity in animal models [26]. ORFV has also shown promise in colorectal cancer models by regulating key processes such as apoptosis, angiogenesis, and cell cycle control [22]. Despite these promising results, further optimization is needed to improve the safety and efficacy of ORFV-based therapies for clinical use.

Recently, wild-type ORFV was found to inhibit the proliferation of nasopharyngeal carcinoma (NPC), a common malignancy in Southeast Asia, southern China, and Hong Kong [23, 27]. This study aimed to investigate the therapeutic potential of two live attenuated ORFVs by comparing their oncolytic effects on two NPC cell lines derived from patients in Hong Kong and Taiwan. Additionally, this study sought to elucidate the underlying mechanisms driving these effects.

Materials and methods

Cell maintenance

Primary goat fibroblasts (FB), a human lung cancer cell line (A549), and a human nasopharyngeal carcinoma cell line (TW02) established from keratinizing squamous cell carcinoma in a Taiwanese patient [28], were cultured in Dulbecco's modified Eagle's medium (DMEM) supplemented with 10% fetal bovine serum (FBS) and 1% penicillin-streptomycin obtained from Gibco BRL (Life Technologies Corporation, Carlsbad, CA, USA). Another human nasopharyngeal carcinoma cell line (HK1) derived from differentiated squamous carcinoma in a patient in Hong Kong [29] was cultured in Roswell Park Memorial Institute (RPMI) medium supplemented with 10% fetal bovine serum (FBS) and 1% penicillin-streptomycin. Both HK1 and TW02 have been verified to be free of Epstein-Barr virus [28, 29], with no concerns regarding HeLa contamination [30]. The NK92 cell line, obtained from ATCC (CRL2407TM), was propagated in alpha-MEM supplemented with 12.5% horse serum (GIBCO, Carlsbad, CA, USA), 12.5% FBS (GIBCO), and 100 U/mL recombinant IL-2 (Sigma-Aldrich, USA). The cells were cultured at 37 °C and 5% CO₂.

Viruses and infection

WT-EGFP (Hoping strain), CBPA-EGFP, and VEGFA-EGFP were cultured in goat fibroblast (FB) cells in accordance with previously described methods [31, 32]. To induce infection, 80% confluent cell monolayers were treated with ORFV at a specified multiplicity of infection (MOI) in infection medium (DMEM without FBS) for 1 h. After allowing for viral adsorption, the infection

medium was replaced with fresh DMEM containing 2% FBS.

Cell viability assays

Propidium iodide (PI) functions as a dye that is incapable of penetrating an intact cell membrane. It exclusively stains the DNA of cells with compromised cell membrane integrity, including those that are deceased or dying [33, 34]. Consequently, the level of PI staining can serve as a marker for cell death or breach of cell membrane integrity. PI staining was avoided in live cells with undamaged cell membranes. Cell viability was assessed by harvesting the cells at 12, 24, or 48 h after infection, followed by centrifugation at $300 \times g$ for 5 min. The supernatant was removed, and the cell pellet was resuspended in PBS. The cells were treated with PI solution (Invitrogen) and incubated at room temperature for 15 min in the dark. A BD Accuri™ C6 flow cytometer was used to analyze the cells that had been stained via flow cytometry (BD Biosciences).

Apoptosis analysis

Apoptotic cells were quantified via a FITC annexin V and PI double-staining apoptosis detection kit (BD Pharmingen™, BD Biosciences). In brief, infected cells were collected at 12 and 24 h after infection and then washed with cold PBS. They were then resuspended in a buffer solution at a concentration of 1 million cells/mL. A total of 100 μ L of the solution containing 1×10^5 cells was added to a mixture of 5 μ L of FITC Annexin V and 5 μ L of PI. The cells were mixed gently via a vortex mixer, incubated for 15 min in the dark, and then analyzed via flow cytometry (BD Accuri™ C6 flow cytometer, BD Biosciences) within 1 h.

Western blot analysis

Proteins were separated via sodium dodecyl sulfate–polyacrylamide gel electrophoresis (SDS–PAGE) and then transferred to a polyvinylidene difluoride (PVDF) membrane. This was followed by immunoblotting with diluted antibodies against the viral proteins F1L, CBP, VEGF (at a dilution of 1:2500, homemade), EGFP (homemade at a dilution of 1:2000), and alpha-tubulin (at a dilution of 1:10,000) overnight at 4 °C. Secondary antibodies, specifically goat anti-mouse or rabbit IgG conjugated with horseradish peroxidase (HRP), were used, and the membranes were incubated with the secondary antibodies for one hour at room temperature. The membrane was washed with 0.05% Tween 20 in PBS, and the signal was detected via an enzyme-linked chemiluminescence assay (SuperSignal; Thermo Fisher Scientific). The intensity of each band was determined by densitometry in ImageJ (NIH) after images were captured via an ImageQuant LAS 4000 (GE Healthcare, Uppsala, Sweden).

NK cell migration assay

The cells were initially infected with viruses, such as WT-EGFP, CBP Δ -EGFP, or VEGF Δ -EGFP, at an MOI of 1 for 24 h. Supernatants from the infected cells were obtained and used as migration-inducing substances. NK92 cells (2×10^5 cells; 100 μ L) were added to the upper well of a transwell filter (Corning; diameter, 6.5 mm; pore size, 5 μ m; 24-well cell clusters). The filters were subsequently positioned in the lower wells, with each well containing 600 μ L of CM. Following a 4-hour incubation of NK92 cells at 37 °C and 5% CO₂, the upper chambers were removed, and the cells that had migrated to the other side of the Transwell membrane were immobilized with methanol, stained with Giemsa solution, and counted under an inverted light microscope.

NK cytotoxicity test (lactate dehydrogenase release-based)

A lactate dehydrogenase [35] release assay was used to assess the cytotoxicity of natural killer (NK) cells against nasopharyngeal carcinoma [27] cells. Briefly, 5000 NPC cells were infected with viruses (e.g., WT-EGFP, CBP Δ -EGFP, or VEGF Δ -EGFP) at an MOI of 1 for 20 h, and NK92 cells were added at ratios of 1:10 and 1:25 (target cells: effector cells) (all samples were analyzed in triplicate). After 4 h of coculture, 50 μ L of the medium was used for the LDH cytotoxicity assay via an LDH cytotoxicity assay kit (Roche, Sigma–Aldrich, USA). The corrected experimental LDH release value was determined by subtracting the spontaneous LDH release value from the effector cells at the corresponding dilutions. NK cell cytotoxicity was defined as follows:

$$\% \text{ cytotoxicity} = \frac{(\text{experimental value} - \text{spontaneous control of effector cells} - \text{spontaneous control of target cells})}{(\text{maximum control of target cells} - \text{spontaneous control of target cells})} \times 100.$$

Plaque assay

FB cells were seeded the previous evening and subsequently infected with serially diluted viruses at a 10-fold concentration. One hour after the adsorption process, the infection medium was replaced with DMEM supplemented with 2.5% FBS and 1.1% methylcellulose. The infection was monitored daily until a cytopathic effect (CPE) was apparent (approximately 14 days). The cells were then treated with 10% formaldehyde and stained with crystal violet.

Generation of stable NPC cells expressing red fluorescent genes

To measure tumor growth accurately, we generated NPC cells expressing a red fluorescent protein (RFP) gene through lentiviral transduction as previously described [36]. NPC HK1 cells were seeded in a 6-well plate and transduced with concentrated lentivirus particles

obtained from RNAiCORE (Academia Sinica, Taiwan). After the cells were incubated at 37 °C for several days, stable NPC cells expressing RFP were selected via puromycin at a concentration of 5 µg/ml. Finally, RFP expression was validated via fluorescence microscopy (Supplementary Fig. 1).

Animal studies

The animal studies were approved by the National Chung Hsing Animal Ethics Committee (IACUC No. 110–106). All procedures were conducted in compliance with the guidelines and regulations. Eight-week-old female nude mice (BioLASCO Taiwan Co., Ltd.) were subcutaneously injected with 1×10^5 HK-1-RFP-expressing cells in the left flank. For this procedure, the mice were anesthetized with 1.5% isoflurane. When the tumors reached a volume of 50 mm³, the mice (8–10 mice/group) were randomly divided into four groups and treated with PBS or (10^6 PFU/100 µL) recombinant orf virus via the intratumoral route once a week for six weeks. Tumor measurements were performed via an in vivo imaging system (IVIS Spectrum, PerkinElmer). The clinical signs of toxicity were closely monitored in the animals until they reached the predetermined sacrifice criteria, which included the tumor burden reaching 10% of their body weight, tumor ulceration, or moribundity.

In vivo imaging system (IVIS)

The fluorescence activity of HK-1-RFP cells in tumor-bearing mice was examined via in vivo imaging studies via a Perkin Elmer IVIS spectrum instrument. To assess the size of the tumors, the mice were anesthetized with isoflurane and placed in a supine position on the IVIS platform at 37 °C. The mice were administered isoflurane via a nose cone, and the camera exposure time was automatically adjusted to *f*/2 with medium binning. The bioluminescence emitted from the whole body or region of interest (ROI) was quantitatively analyzed via Living Image® software (version 3.0) by measuring the luminescence signal intensity in photons per second (photons/s), with the ROI settings applied [37, 38]. The ROI was determined by measuring the total flux of photons and focused on the left flank region of the tumor site via whole-body imaging.

Histopathology and immunohistochemistry (IHC)

Tumor samples were fixed in 10% formalin and embedded in paraffin wax. The samples were then cut into 3 µm thick sections, mounted on glass slides, and stained with hematoxylin and eosin following a previously described method [39]. The necrosis score was evaluated by three qualified pathologists. The severity of necrosis was graded according to the method described by Shackelford et al. [40]. The degree of necrosis was assessed on a scale

of one to five, with the severity ranging from minimal (<1%) to severe (76–100%). The grading scale was as follows: “1” indicated minimal necrosis (<1%), “2” indicated slight necrosis (1–25%), “3” indicated moderate necrosis (26–50%), “4” indicated moderate to severe necrosis (51–75%), and “5” indicated severe necrosis (76–100%).

For the immunohistochemical analysis, the homemade polyclonal antibody “F1L” was utilized with the DakoEn-Vision+HRP Kit (Dakopatts, Glosstrup, Denmark), which employs a two-step peroxidase method. The tissue sections were deparaffinized and washed in Tris-buffered saline (TBS). The cells were then treated with 1% hydrogen peroxide in TBS for 20 min to inactivate endogenous peroxidases. After being washed, the sections were treated with 2% bovine serum albumin (BSA) in TBS for 10 min, followed by an overnight incubation with the primary antibody at 4 °C. The primary antibody was diluted 1:1000 in TBS containing 1% BSA. Duplicate sections were used as negative controls and were incubated with 2% BSA instead of the primary antibody. After the sections were washed in TBS three times for 5 min each, they were incubated with peroxidase-conjugated goat anti-rabbit secondary antibody for 30 min. The sections were then washed with TBS, and peroxidase activity was visualized by incubating them in TBS containing 0.06% DAB (Sigma–Aldrich) and 0.034% hydrogen peroxide for 2 min. Finally, the sections were washed with tap water, counterstained with Mayer’s hematoxylin, and mounted with Entellan (Merck, Darmstadt, Germany).

Statistical analysis

The data are presented as the means ± standard errors of the means and were analyzed via GraphPad Prism version 8.0 (GraphPad Software, Inc.). Student’s *t* test was used to assess whether the differences between the two groups were statistically significant when their means were compared. To evaluate differences between multiple groups, one-way analysis of variance (ANOVA) was conducted, along with post hoc tests using Tukey’s multiple comparisons test to determine statistical significance. Two-way repeated-measures ANOVA was used to examine tumor volume in multiple groups at various time points, and Dunn’s multiple comparison test was used as a post hoc test to assess significant differences among the treatment groups during tumor treatment. A *p* value less than 0.05 was considered indicative of statistical significance.

Results

Cytotoxicity and replication kinetics of ORFV (hoping strain) in two NPC cell phenotypes

ORFV (NA1/11) can effectively kill NPC cells (e.g., CNE-2, 5–8 E, and HONE-1) [23]. Several strains of ORFVs with various characteristics are present in circulation within the natural environment [41–44]. Moreover, the

clinicopathological characteristics of nasopharyngeal carcinoma [27] that are currently observed across various studies in Asia are variable. Furthermore, the effects of wild-type ORFV (TW/Hoping strain) expressing EGFP (WT-EGFP) were evaluated in two NPC cell lines, TW02 and HK1, which exhibit different histological characteristics and are derived from patients in Taiwan and Hong Kong, respectively [28, 29]. Both cell lines are free of genomic contamination [30] and have been extensively studied in previous research, covering topics from tumor cell motility [45, 46] to tumor innate immunity [47–49]. For comparison, two positive cell lines were used: a goat fibroblast (FB) line, which represents the authentic animal host, and a human lung carcinoma cell line (A549), recognized as the most permissive human cancer cell line for ORFV [21].

As anticipated, WT-EGFP effectively infected the goat FB cells (Fig. 1A). Notably, infection levels in both NPC cell lines, HK1 and TW02, were significantly greater than those in the positive control cancer cells (A549) (Fig. 1). Notably, the NPC-HK1 cell phenotype was more susceptible to WT-EGFP than TW02 24 h post infection (hpi), as evidenced by the green fluorescence (EGFP) signal observed via microscopy (Fig. 1A) and the accumulation of the major viral envelope F1L protein (Fig. 1B and C). Furthermore, the production of viral progeny was noticeably greater in HK1 cells than in TW02 NPC cells. (Fig. 1D and E).

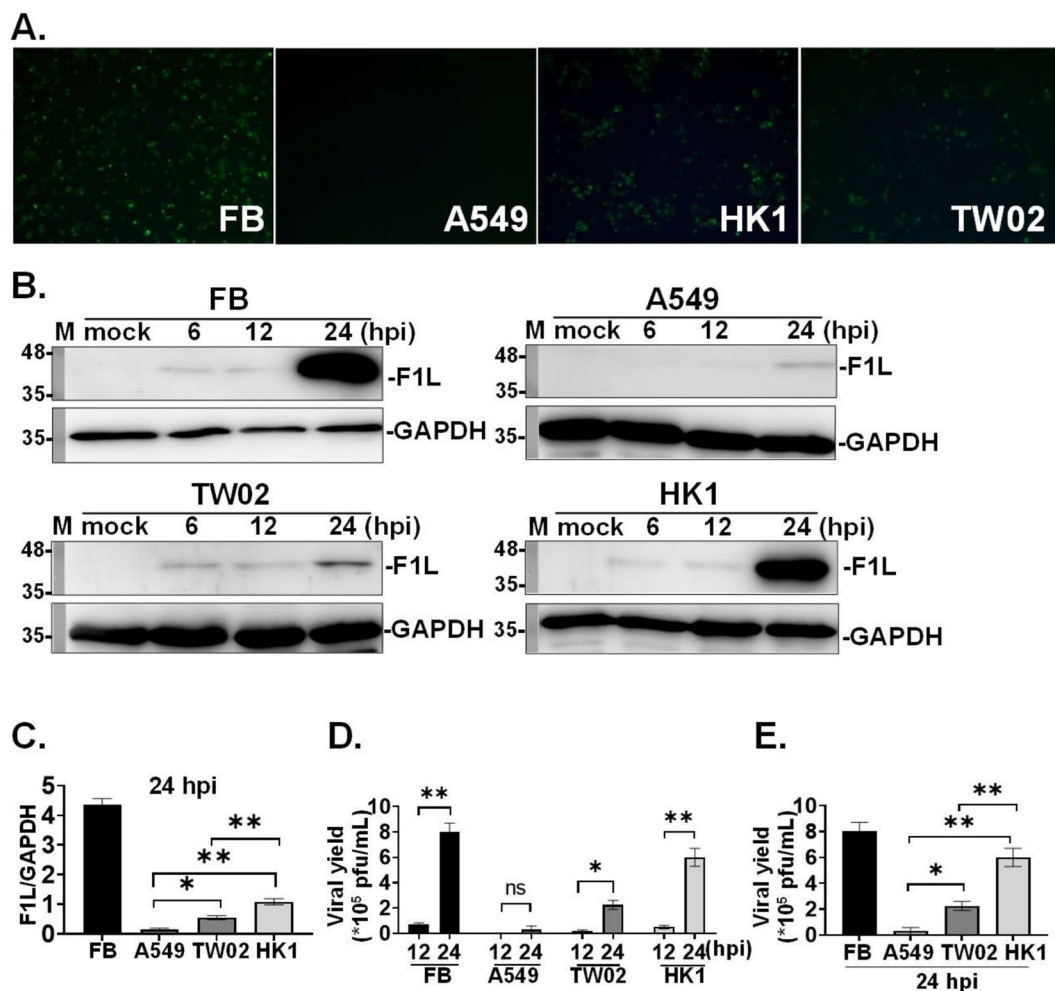


Fig. 1 Susceptibility of the two NPC phenotypes to ORFV. Two NPC cell lines (HK1 and TW02), together with goat FB and A549 cells (positive control cancer cells), were infected with the WT-EGFP virus at an MOI of 0.5. The expression of the reporter gene was directly visualized via fluorescence microscopy at 24 h post infection (hpi) (A). The protein expression profile and yield of virus progeny in cells infected with WT-EGFP at specific time points were determined by western blot analysis (B and C) and plaque assays (D and E), respectively. One-way ANOVA and post hoc tests with Tukey's multiple comparisons were performed (C and E), and significant differences in the mean viral F1L protein or viral yields at 24 hpi between the groups were considered significant at * $p < 0.05$, ** $p < 0.01$, and *** $p < 0.001$. "n.s." indicates no significance. Student's t test was performed (D), and significant differences in the mean viral F1L protein or viral yields between the groups were considered significant at * $p < 0.05$, ** $p < 0.01$, and *** $p < 0.001$. "n.s." indicates no significance

Characterization of cell death induced by WT-EGFP in NPC cells

Next, we determined whether ORFV infection induces cell death in NPC cells. Indeed, WT-EGFP induced

approximately 20% and 13% cell death at 24 hpi in HK1 and TW02 cells, respectively (Fig. 2A). However, this was not attributed to activated apoptotic pathways, as indicated by negative Annexin V staining, even at 24 hpi

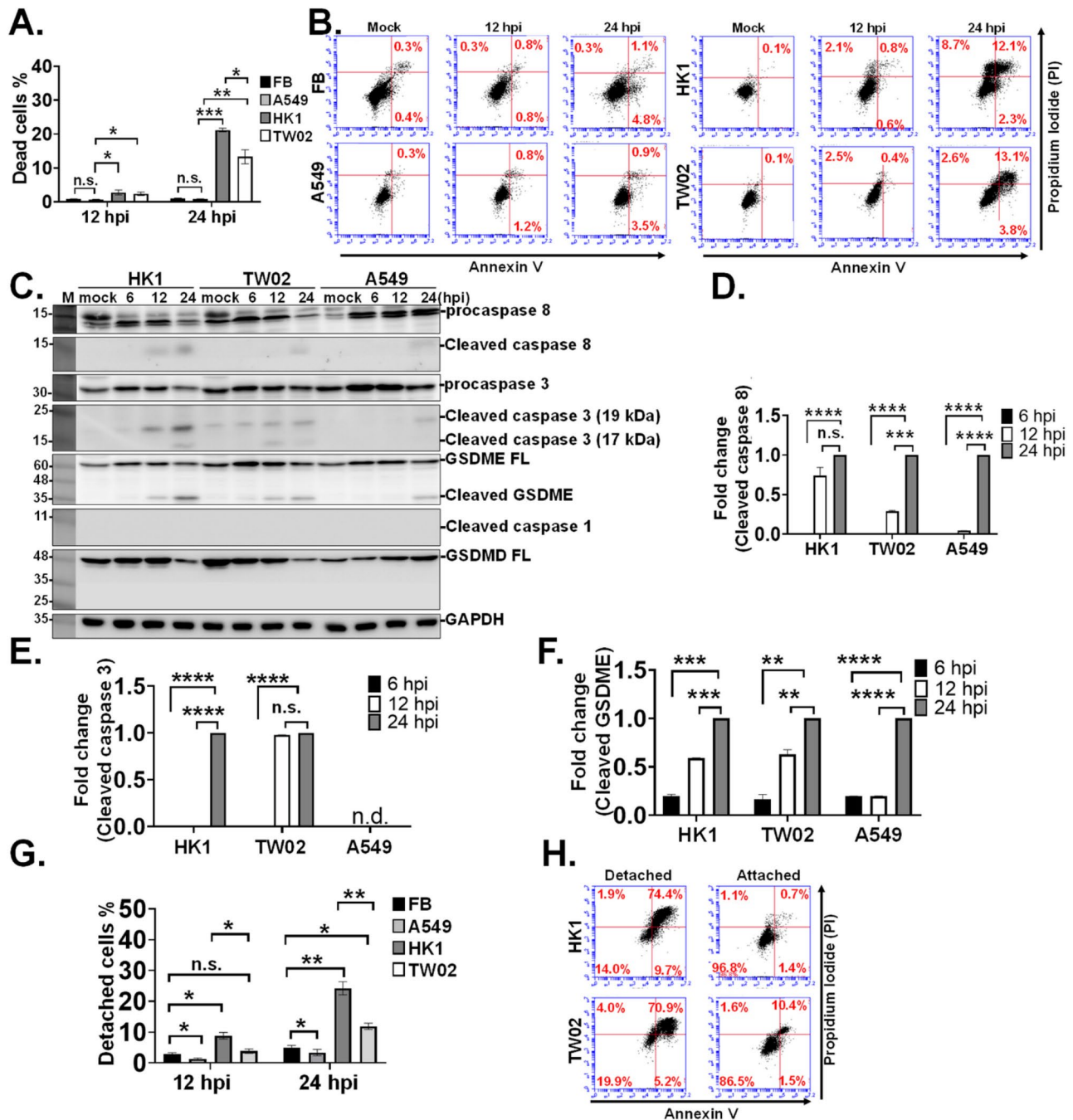


Fig. 2 Characterization of NPC cell death induced by the WT-EGFP virus. Four types of cells were infected with the WT-EGFP virus at an MOI of 0.5. Overall cell death was initially measured by propidium iodide (PI) staining at 12 and 24 hpi (A). Moreover, the progression of ORFV-induced cell death, such as apoptosis, was determined by double staining with Annexin V and PI (B). The protein expression profile indicating the mechanism of cell death (e.g., apoptosis or pyroptosis) was determined by western blot analysis (C), and the results are plotted (D, E, F). The Western blotting results were normalized to the values at 24 hpi. The percentage of detached cells after ORFV infection was monitored (G). The status of the attached and detached NPC cell populations was further evaluated by annexin V/PI double staining (H). One-way ANOVA and post hoc analysis via Tukey's multiple comparisons were performed, and significant differences between groups were considered significant at * $p < 0.05$, ** $p < 0.01$, *** $p < 0.001$, and **** $p < 0.0001$. "n.s." indicates no significance. "n.d." indicates that no protein was detected

(Fig. 2B). Recently, it was reported that ORFV can induce pyroptosis in EMT6, an epithelium-derived murine breast cancer cell line [25]. Therefore, we explored ORFV-induced pyroptosis in NPC cells. The involvement of pyroptosis-related genes (*Gsdmd*, *Casp1*, *Casp8*, *Casp3*, and *Gsdme*) was examined. Notably, cleaved caspase 1 was not detected in the NPC or A549 cell lines (Fig. 2C). Notably, cleaved gasdermin D (GSDMD) (GSDMD-N), which acts as a downstream signaling molecule of cleaved caspase 1, was not detected (Fig. 2C). In contrast, as early as 12 hpi, noncanonical pyroptosis-related proteins, including gasdermin E (GSDME), caspase 3, and caspase 8, were cleaved after infection, particularly in HK1 cells (Fig. 2C-F). Additionally, compared with the effects of the virus on A549 and FB cells, WT-EGFP infection resulted in a considerable increase in the detachment of NPC cells, with approximately 20% detachment in HK1 cells and 10% detachment in TW02 cells (Fig. 2G). To determine the viability status of the HK1 and TW02 cell populations, especially the detached cells after WT-EGFP infection, we performed annexin V-propidium iodide (PI) staining. The current data revealed that approximately 70% of the detached HK1 cells died, as evidenced by PI-positive staining (Fig. 2H). Overall, these findings suggest that ORFV infection

induces detachment and triggers noncanonical caspase-dependent pyroptosis in NPC cells via GSDME cleavage.

The replication kinetics and cytotoxic effects of attenuated ORFs are similar to those of WT-EGFP in NPC cells

A previous study demonstrated that deletion of the viral gene encoding a chemokine binding protein (CBPΔ-EGFP) or vascular endothelial growth factor (VEGFΔ-EGFP) significantly attenuated ORFV (TW/Hoping strain) in its natural host animal [31]. Hence, the oncolytic potential of these deletion mutant viruses against two NPC cell lines was evaluated. HK1 and TW02 cells, along with positive control A549 cells, were treated with WT-EGFP, CBPΔ-EGFP, or VEGFΔ-EGFP. The ability of the deletion mutant viruses to eliminate tumor cells (as shown in Fig. 3A and B) and facilitate viral replication (as demonstrated in Fig. 3C and F) was compared with that of the wild-type EGFP viruses. The levels of the F1L protein and EGFP reporter protein expressed by the viruses decreased substantially in all tumor cells infected with VEGFΔ-EGFP and CBPΔ-EGFP at 48 h postinfection (hpi) compared with those in those infected with WT-EGFP, as shown in Fig. 3A and B. In line with the F1L levels, VEGFΔ-EGFP produced the least amount of viral progeny among the three viruses examined in all the

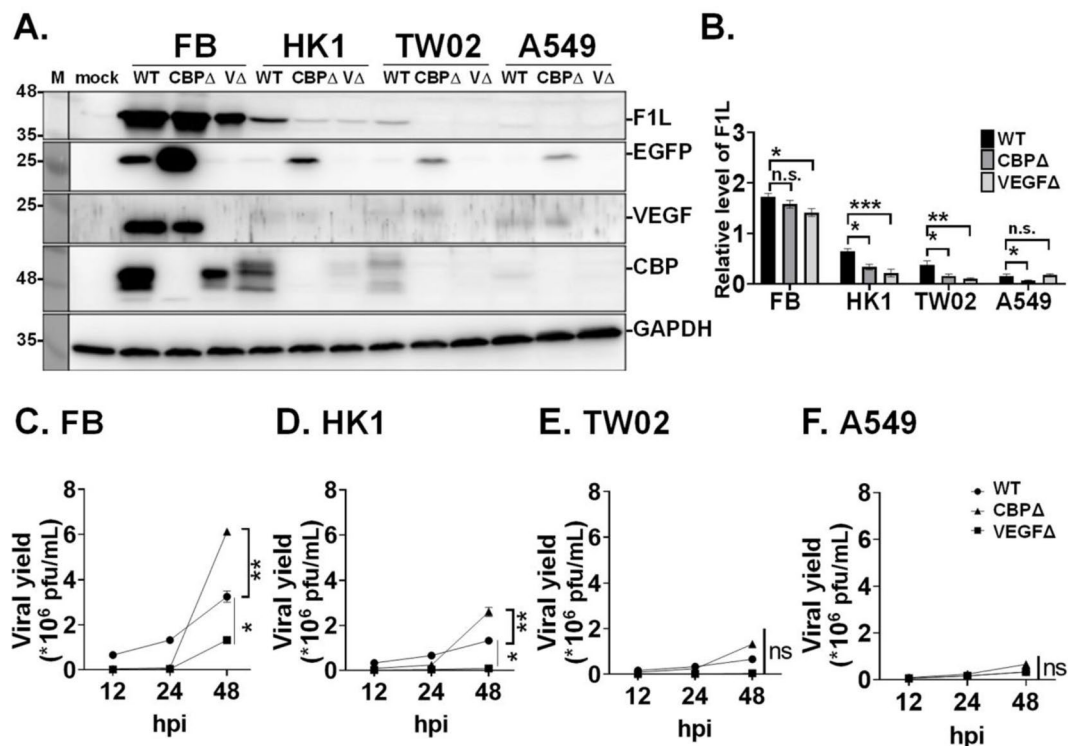


Fig. 3 Susceptibility of the two NPC phenotypes to two recombinant ORFs. Four cell types, as indicated, were infected with WT-EGFP or the other two recombinant ORFs, including CBPΔ-EGFP and VEGFΔ-EGFP, at an MOI of 0.5. The protein expression profile and yield of virus progenies in cells infected with recombinant viruses at specific time points were determined via western blot analysis (A and B) and plaque assays (C, D, E, and F), respectively. One-way ANOVA and post hoc analysis with Tukey's multiple comparisons were performed, and significant differences in the viral F1L protein or viral yields between groups were considered significant at * $p < 0.05$, ** $p < 0.01$, and *** $p < 0.001$. "n.s." indicates no significance

cell lines and at all the time points (Fig. 3C-F). Interestingly, compared with WT-EGFP, CBPΔ-EGFP resulted in a lower titer at 24 hpi, but at 48 hpi, viral production was significantly greater and exceeded that of WT-EGFP (Fig. 3C-F), which aligns with the fluctuating expression levels of EGFP (Fig. 3A).

Characterization of cell death induced by ORFVs in NPC cell lines

To evaluate the capacity of attenuated ORFV to cause cell death, we initially investigated the degree of cell death initiated by these two attenuated viruses in three distinct cancer cell lines and found that HK1 cells presented the highest susceptibility to all recombinant orf viruses, resulting in approximately 33–42% cell death in all infected groups, followed by TW02, with 23–36% cell death. In contrast, A549 cells presented a significantly lower percentage of cell death (0.2–2%) after ORFV infection (Fig. 4A). Nevertheless, among the recombinant viruses, VEGFΔ-EGFP caused significantly less cell death than did CBPΔ-EGFP and WT-EGFP.

To verify whether the cell death caused by recombinant ORFVs in NPC cell lines was attributed to pyroptosis, we conducted further analyses. Similarly, attenuated ORFVs did not execute the canonical pathway for pyroptosis, as shown by the undetectable levels of cleaved caspase 1 and GSDMD-N in the western blot analysis (Fig. 4B). Instead, the data revealed that GSDME was cleaved in NPC cells infected with either wild-type ORFV or two attenuated ORFVs (Fig. 4B and E), which was correlated with the activation status of Caspase-8 and Caspase-3, the upstream events of GSDME cleavage (Fig. 4B-D). The overall expression of GSDME in ORFV-infected cells was greater than that in mock control cells (Fig. 4B). However, there were no significant differences in the levels of cleaved GSDME (activation) among the three ORFVs analyzed (4B and E). In summary, attenuated ORFV viruses induce the same type of cell death in tumor cell lines, regardless of their attenuated nature.

Notably, 30–50% cell detachment was observed in the infected groups, particularly in the WT and CBP-defective mutants, 48 h after infection (Fig. 5A). The activation status of focal adhesion kinase (FAK) and protein kinase B (AKT) was assessed, as these signaling molecules play crucial roles in cell attachment [50] and survival [51], respectively. Our findings demonstrated that infection with wild-type ORFV significantly reduced FAK expression and AKT phosphorylation in both HK1 and TW02 cells (Fig. 5B). Moreover, FAK and AKT phosphorylation levels were significantly lower in mutant ORFV-infected NPC cells than in mock-treated cells (Fig. 5B-D). Therefore, in addition to GSDME-mediated pyroptosis, ORFV infection may lead to NPC cell death via the inhibition of the FAK and AKT signaling pathways.

NK cells enhance oncolytic ORFV cytotoxicity in NPC cells

Oncolytic virotherapy triggers an antitumor response that is significantly influenced by natural killer (NK) cells [52–54]. Therefore, we assessed the capacity of ORFV to stimulate NK cells and promote NPC cell death. The ratio of the number of NK cells to the number of NPC cells, known as the effector-to-target (E: T) ratio, is typically regarded as a significant factor in population-based studies because of its impact on NK cell cytotoxicity [55]. As demonstrated in Fig. 6A, TW02 cells that had been infected and cocultured with NK cells displayed a significantly greater level of cell death in a dose-dependent manner than those that were treated with either the virus or the NK cells alone. However, among the three recombinant viruses, the cytotoxic ability of both null mutants was significantly lower than that of the WT ORFV. This phenomenon was consistently observed in HK1 cells (Fig. 6B).

OVs are highly effective at recruiting an arsenal of immune components, including NK cells. Therefore, we evaluated the effect of ORFVs on NK cell chemotaxis. Using a Transwell migration assay [56], we determined whether conditioned media from NPC cells (TW02 and HK1) infected with recombinant ORFV could induce NK cell chemotaxis. Compared with mock infection, conditioned media from both WT-EGFP- and VEGFΔ-EGFP-infected HK1 cells increased the migration of NK cells to the lower chamber (Fig. 6C and D). An increase in conditioned media-driven NK chemotaxis was also observed in TW02 cells infected with WT-EGFP or VEGFΔ-EGFP (Fig. 6C and D).

Overall, WT-EGFP and VEGFΔ-EGFP infection significantly promoted NK cell chemotaxis. The inclusion of natural killer (NK) cells significantly enhanced the cytotoxic activity against HK1 and TW02 target cells, an effect triggered by ORFV infection.

Evaluation of the therapeutic efficacy of recombinant ORFV in a xenograft NPC model

To evaluate the effect of recombinant ORFVs on tumor growth, we utilized a mouse model of NPC (HK1) cells because of their high sensitivity to ORFV infection. Moreover, to facilitate the measurement of tumor growth, we generated reporter-HK1 cells expressing red fluorescent protein (RFP) via lentivirus transduction. The homogeneity of HK1-RFP cells was confirmed via a fluorescence assay (Supplementary Fig. 1).

In this study, 1×10^5 RFP-expressing HK1 cells were subcutaneously engrafted into the left flank of nude mice. On day 14 post-tumor transplantation, when the tumor size appeared uniform among the groups, PBS or individual recombinant ORFV (10^6 PFU in 100 μ L) was inoculated into the tumor. The dose regime is shown in Fig. 7A. The fluorescence signal in the PBS-treated mice

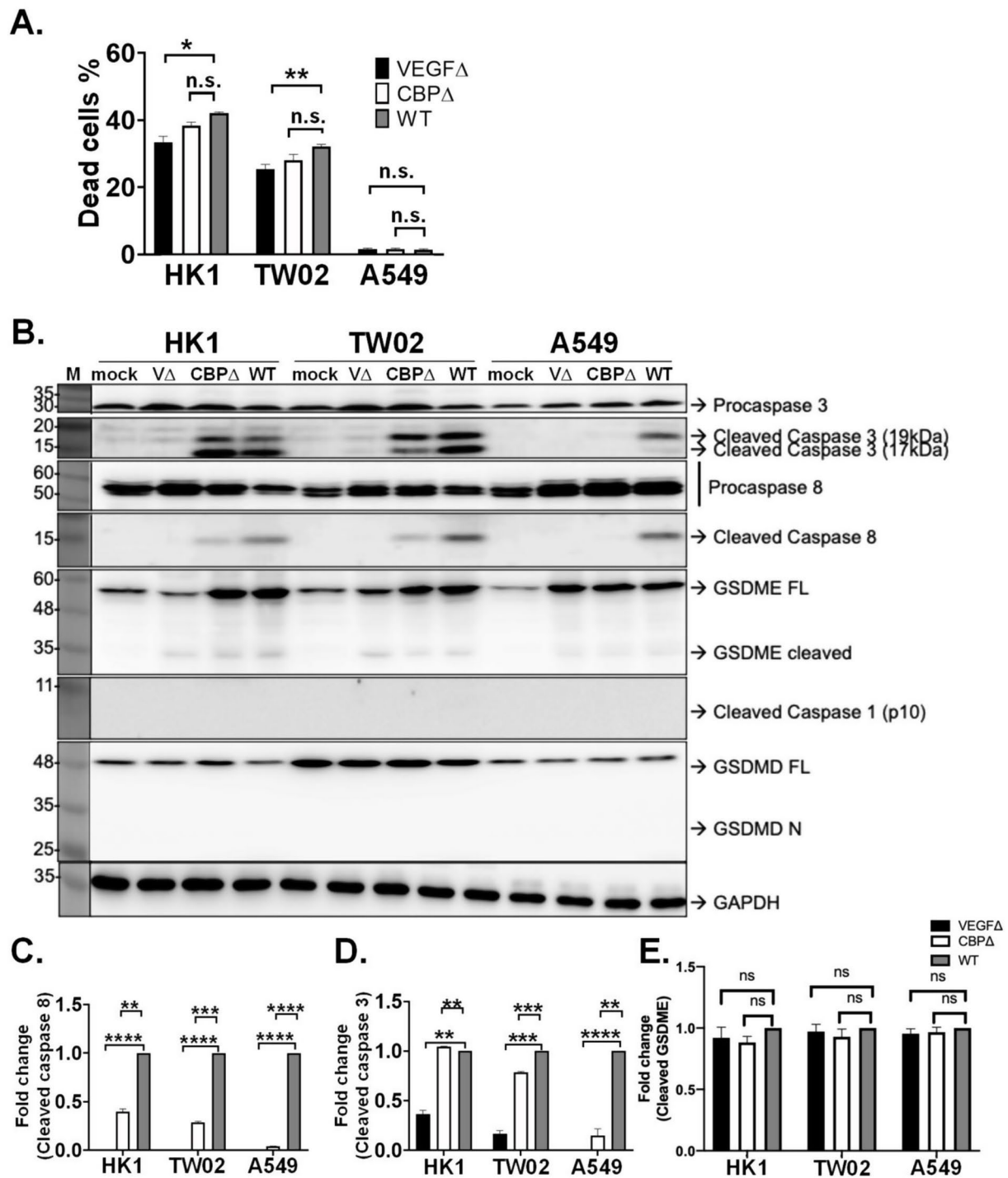


Fig. 4 Characterization of cell death induced by recombinant ORFVs in two cell phenotypes of NPC. The cells were infected with WT-EGFP, CBP Δ -EGFP, or VEGF Δ -EGFP at an MOI of 0.5. The percentage of cell death was measured by PI staining (**A**). The expression of markers of pyroptosis was determined by western blot analysis (**B**), and the relative activation levels of caspase 8, caspase 3 and GSDME were estimated and plotted (**C-E**). One-way ANOVA and post hoc analysis with Tukey's multiple comparisons were performed, and significant differences between groups were considered significant at * $p < 0.05$, ** $p < 0.01$, *** $p < 0.001$, and **** $p < 0.0001$. "n.s." indicates no significance

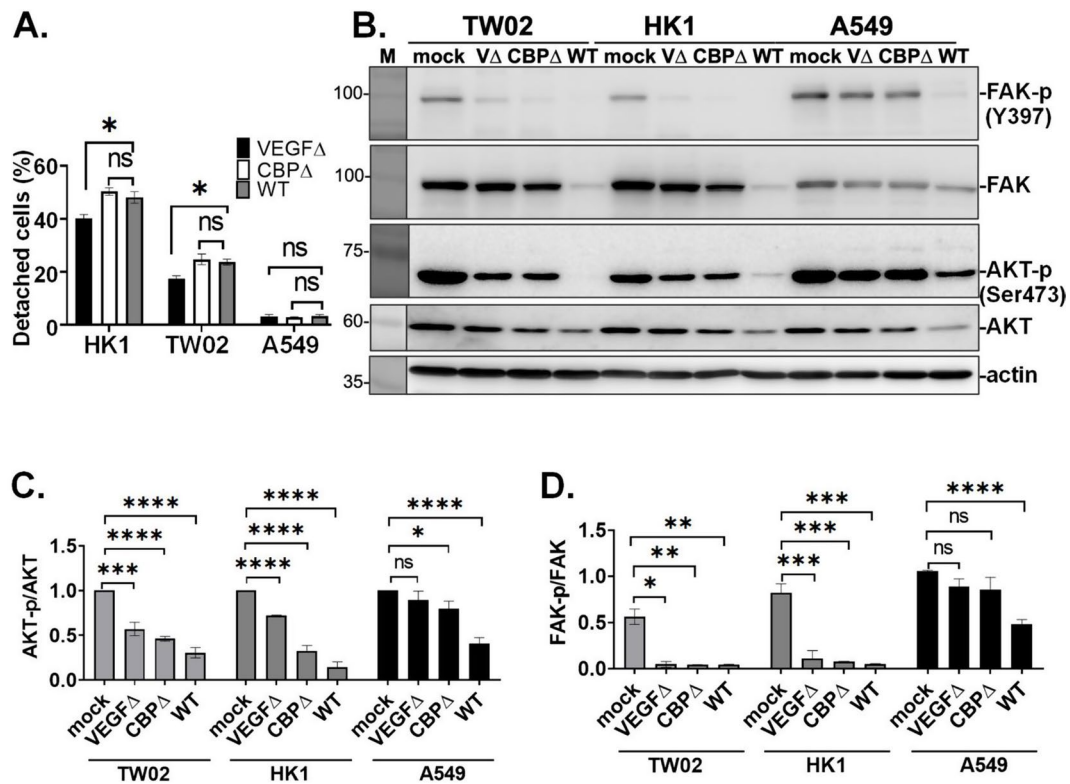


Fig. 5 ORFV infection suppresses FAK and AKT signaling activation in NPC cells. The cells were infected with ORFV, WT-EGFP, CBPΔ-EGFP, or VEGFΔ-EGFP at an MOI of 0.5. The percentage of detached cells was estimated at 48 hpi (A). The expression of proteins responsible for cell detachment and survival (FAK and AKT) was detected by western blot analysis (B), and their relative activation levels are plotted (C, D). One-way ANOVA and post hoc analysis with Tukey's multiple comparisons were performed, and significant differences between groups were considered significant at $*p < 0.05$, $**p < 0.01$, $***p < 0.001$, and $****p < 0.0001$. "n.s." indicates no significance

increased dramatically until the end of the experiment, whereas the tumor growth rate in the ORFV-treated mice showed an overall slow increase that was undetectable in some mice (Fig. 7B-F). Interestingly, a significant decrease in tumor size between the groups treated with WT-EGFP and CBPΔ-EGFP was observed as early as 1 week posttreatment compared with that in the PBS-treated group (Fig. 7C) but not in the group treated with VEGFΔ-EGFP (Fig. 7D). Additionally, a substantial reduction in tumor size was observed in the groups that received WT-EGFP and CBPΔ-EGFP treatments at 6 weeks posttreatment, but this reduction was not observed in the VEGFΔ-EGFP group (Fig. 7E and F). This may be due to the viral treatment of a single mouse in the VEGFΔ-treated group that developed tumor ulceration, which hindered the antitumor efficacy of the viral treatment. The removal of this mouse resulted in a substantial reduction in the tumor volume of the mice that received treatment with VEGFΔ-EGFP (Supplementary Fig. 2).

Six weeks after treatment, all the mice were sacrificed, and histopathological examination was performed to assess tumor necrosis. Individual cell keratinization and keratin pearl formation, highlighted by dotted boxes, were observed in all the samples (Fig. 8A-D). Moreover,

keratohyalin granules were found in virus-infected tumors, as indicated by the arrows (Fig. 8F-H). In particular, tumors treated with recombinant ORFV presented moderate to severe necrosis, whereas those in the PBS-treated group presented moderate tumor necrosis (Fig. 8A-D and N). Notably, there was an increase in the number of tumor-infiltrating lymphocytes and neutrophils and fewer viable NPC cells in tumors treated with WT-EGFP and the two deletion mutants (Fig. 8F-H). Conversely, tumors treated with PBS had fewer infiltrating lymphocytes and inflammatory cells (i.e., neutrophils) and a greater number of viable NPC cells (Fig. 8E).

To determine whether infection with recombinant viruses was responsible for the oncolytic effect, immunohistochemical staining and polymerase chain reaction (PCR) were conducted to confirm the presence of ORFV in tumor tissues. As shown in Fig. 8I-L, the F1L antigen was present in the ORFV-infected tumor samples but not in the control samples. Similarly, the viral B2L gene was readily detected in the infected tumors even six weeks after inoculation (Fig. 8M). The presence of viral protein (F1L) and DNA in infected tumors indicated a correlation between tumor suppression and ORFV infection in NPC xenograft models.

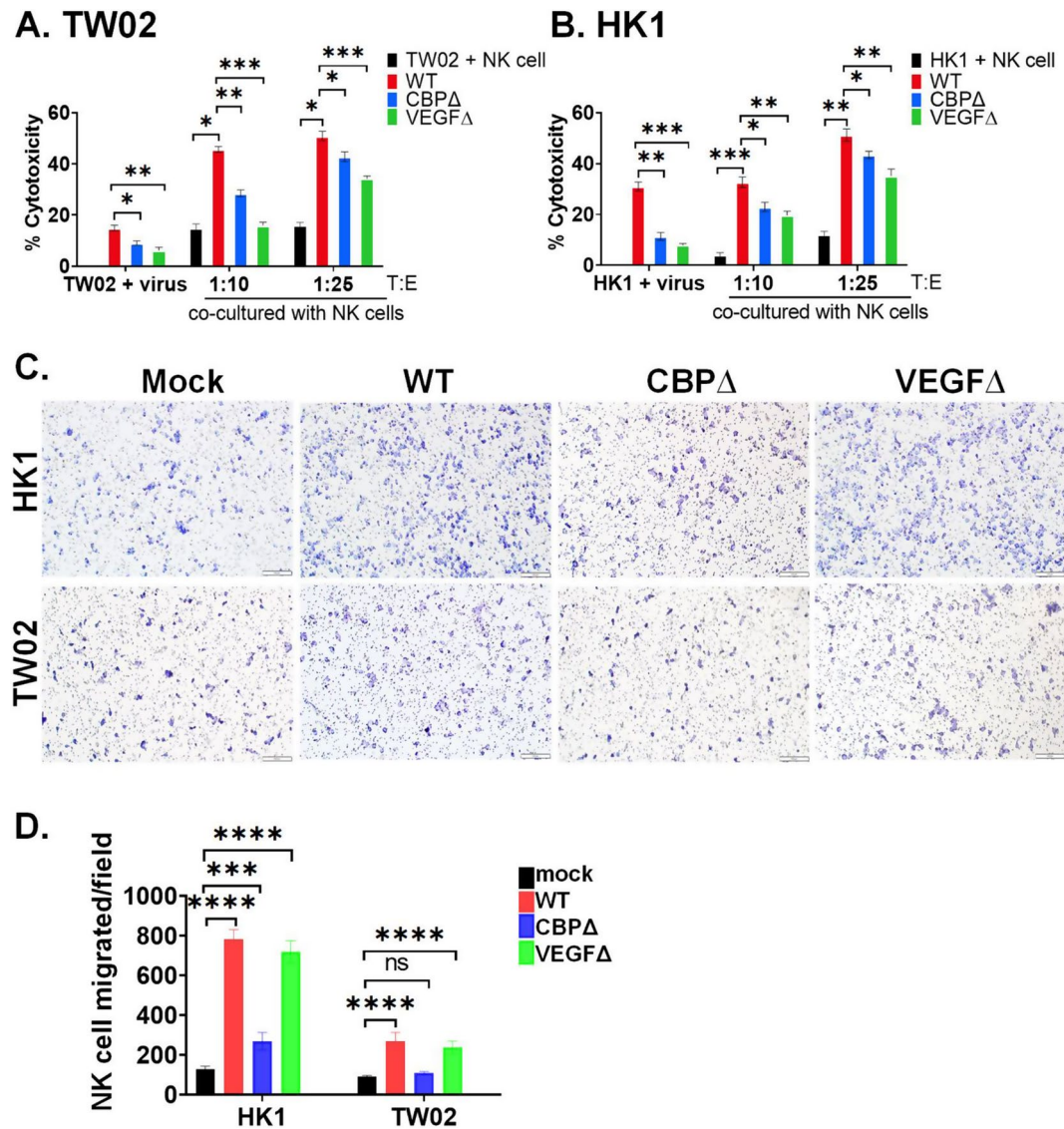


Fig. 6 NK cells augment oncolytic ORFV cytotoxicity in NPC cells. TW02 and HK1 cells (as target cells) were cocultured with effector NK cells at different ratios of effector cells to target cells (E:T), followed by infection with either WT or deletion mutant viruses at an MOI of 1. The viability of TW02 and HK1 cells was determined via an LDH release assay and plotted (**A** and **B**, respectively). Moreover, a Transwell migration assay was performed to estimate the migration of NK cells, as described in the Materials and Methods section. Briefly, the infected cell supernatant served as the conditioned medium for the NK cells seeded in the upper chamber. After 4 h of incubation, the number of NK cells that migrated through the membrane and into the lower chamber was recorded (**C**) and measured (**D**). One-way ANOVA and post hoc analysis with Tukey's multiple comparisons were performed, and significant differences between groups were considered significant at $*p < 0.05$, $**p < 0.01$, $***p < 0.001$, and $****p < 0.0001$. "n.s." indicates no significance.

Discussion

Oncolytic viruses (OVs) selectively replicate in cancerous cells, elicit strong immune responses [16], and have been regarded as alternative treatment strategies for tumors that are resistant to immunotherapy alone [57]. ORFV exhibits oncolytic activity in various human cancer cell lines [21, 22, 25, 58], including NPC [23]. However, the use of zoonotic viruses in cancer therapy raises safety concerns. To improve the safety of medical applications, we generated two attenuated ORFVs (VEGFΔ-EGFP and CBPΔ-EGFP) by removing the virulence factor [31]. The

current study further demonstrated that wild-type (WT-EGFP) and the two attenuated ORFVs exerted oncolytic effects on NPC cell lines derived from patients in Taiwan and Hong Kong. Moreover, the suppression of NPC by attenuated ORFV infection was demonstrated for the first time in a murine xenograft model.

ORFV targets epithelial cells [59], making it an ideal OV for NPC treatment. Numerous studies have shown significant variations in the sequences of ORFV strains [31, 60–62]. For example, a comparison between the VEGF gene in our local strain (TW/Hoping) and the

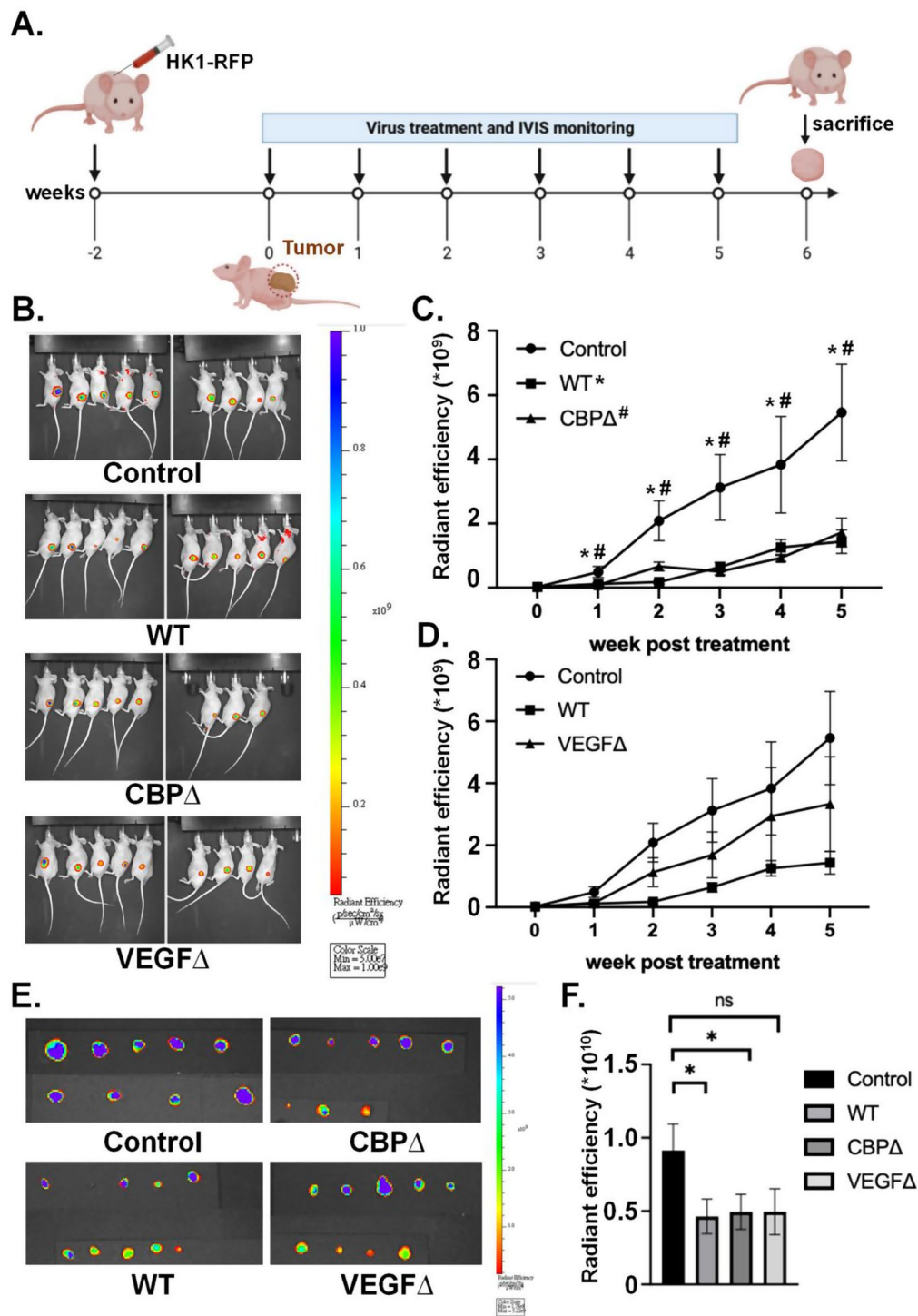


Fig. 7 Efficacy of ORFV infection against tumor growth. **(A)** Schematic diagram of the ORFV treatment schedule. The mice were injected subcutaneously with HK1-RFP cells and then treated with RPMI medium (mock control), WT-EGFP, or one of the recombinant viruses (VEGFΔ or CBPΔ) at 10^6 pfu/100 μ L once a week for six weeks. The tumor size was monitored via the IVIS Spectrum imaging system **(B)**, and the relative size was plotted **(C and D)** via the ROI settings of Living Image[®] 3.0 [37, 38]. After the mice were sacrificed, the tumors from each mouse were removed, and their size was measured via IVIS **(E)** and plotted **(F)**. Two-way repeated-measures ANOVA and post hoc analysis with Dunn's multiple comparison test were performed **(C and D)**, and significant differences between groups were considered significant at * or # $p < 0.05$. "n.s." indicates no significance. One-way ANOVA and post hoc analysis with Tukey's multiple comparisons were performed **(F)**, and significant differences between groups were considered significant at * $p < 0.05$. "n.s." indicates no significance

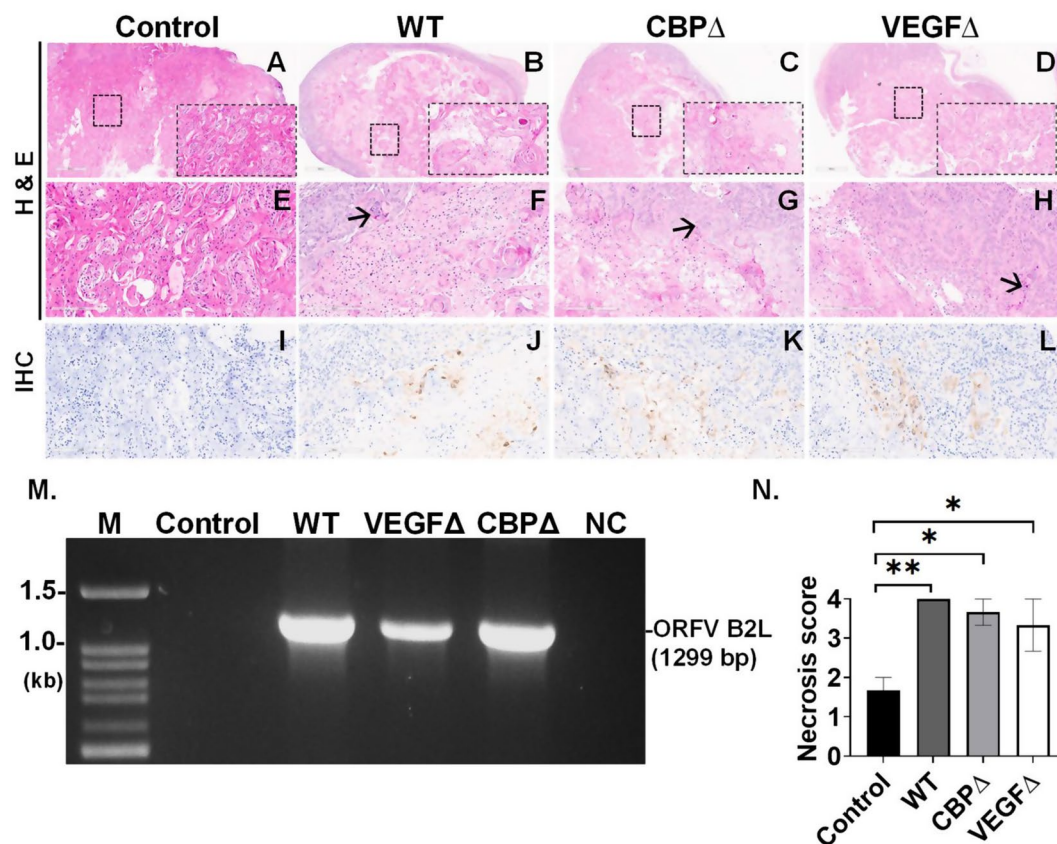


Fig. 8 Pathological examination of tumors in mice infected with ORFVs. Histopathological examination was performed by staining the tumor tissue sections with hematoxylin and eosin (H&E) (A–H). Moreover, ORFV infection in tumors was monitored by the presence of a viral protein (F1L) and a genome (B2L gene) in tissue samples via immunohistochemical staining with an F1L antibody (I–L) and PCR (M). Individual cell keratinization and keratin pearl formation (marked by a dotted box and zoomed-in images are shown in the inset boxes) were observed. Keratohyalin granules were found in virus-infected tumors, as indicated by arrows (F–H). Tissue necrosis and infiltration of tumor lymphocytes were also noted (E–H). The necrotic scores of the different groups are shown (N). One-way ANOVA and post hoc analysis with Tukey's multiple comparisons were performed, and significant differences between the treatment groups were considered significant at * $p < 0.05$ and ** $p < 0.01$. "n.s." indicates no significance

NA1/11 strain, which is commonly used to assess the oncolytic effects of ORFV in NPC [23], revealed a difference of 45.73% [31]. Consequently, the results obtained from the NA1/11 strain in a previous study may not accurately represent the fundamental mechanism of our locally isolated strain from goats. NPC cell lines with different phenotypes, such as CNE-2, 5–8 E, and HONE-1, have been used to elucidate the oncolytic activity of ORFV in NPC [23]. The susceptibility of cell phenotypes to the same virus varies owing to factors such as cellular receptors, intracellular defense mechanisms, and viral replication ability [63]. Differences in innate immune responses, cellular permissiveness, lifespan, turnover, communication between cells, and tissue-specific factors also contribute to the differences in susceptibility observed among various cell phenotypes when exposed to the same virus [64–66]. Understanding these variations is crucial for studying viral pathogenesis and for developing virus-based targeted therapies. In this study,

we demonstrated that HK1 cells were more susceptible to ORFV than TW02 cells were (Fig. 1), suggesting that the effects of OV may depend on cell-specific factors. For instance, HK1 cells express significantly higher basal levels of pro-IL-1 β compared to TW02 cells [49]. Derived from patients with undifferentiated NPC, HK1 cells exhibit high tumorigenic potential and invasive properties [29]. Furthermore, HK1 cells express high levels of the oncogene *c-Met*, which is linked to the promotion of cancer cell growth, survival, and invasion [29]. Overall, differences in the phenotypic characteristics of TW02 and HK1 cells may affect their responses to treatment regimens, such as oncolytic viruses, highlighting the importance of using appropriate cell lines for preclinical studies. For ease of tumor size measurement, a reporter HK1 cell line expressing the fluorescent RFP protein was established in this study (Supplementary Fig. 1). Owing to the unsynchronized growth of TW02 tumors, in our preclinical studies, only reporter HK1 cells were selected

to establish a xenograft model in nude mice, and an IVIS was utilized to observe tumor growth.

After entering a host cell, viruses regulate programmed cell death and/or evade surveillance by the immune system to establish early infection. Various forms of cell death, such as apoptosis, necrosis, necroptosis, pyroptosis, and autophagic cell death, are induced by OV_s to eliminate both cancer and cancer-associated endothelial cells [67]. Typically, one type of cell death is predominant for each OV. The interaction of the immune system with oncolytic viruses highlights the potential of replicating viruses as immunotherapeutic agents for cancer treatment [68]. ORFV induces cell death via autophagy [23] and apoptosis [22]. However, our study revealed that ORFV infection induced cell death via the caspase-dependent noncanonical pyroptosis pathway, in which cleaved GSDME, rather than GSDMD, was detected in ORFV-infected cells (Fig. 2B). Moreover, as shown in Fig. 4, despite the attenuated nature of the two deletion viruses, their capacity to induce cell death in NPC cells remained intact and consistent through the same mechanism as that of the WT virus, which involved caspase-dependent GSDME cleavage. The activation of GSDME in NPC cells was attributed mainly to caspase-8 activity, accompanied by caspase-3 activation (Fig. 2C-E). This finding is consistent with a report by Lin et al., in which the ORFV strain OV-SY17 induced GSDME-mediated pyroptosis to activate antitumor immunity in several cell lines [25]. In addition, several lines of evidence have indicated that viruses can induce pyroptosis in healthy cells. For example, influenza A and vesicular stomatitis viruses are known to induce pyroptosis in epithelial cells and bone marrow-derived macrophages, respectively [69, 70]. It has been suggested that dying cells release molecular components such as the high-mobility group B1 (HMGB1) protein [71], which can be identified as DAMPs and act as danger signals to trigger immunogenic cancer cell death (ICD). HMGB1 contributes to the maturation and antigen uptake of dendritic cells, which are subsequently presented to the immune system [72]. Additionally, it can act as a powerful immunological adjuvant to activate the cytotoxic T lymphocyte response [73]. Hence, manipulating the ICD is a new strategy to improve the effectiveness of cancer treatment.

A significant advantage of OV_s as cancer treatments is their ability to target pathways that facilitate tumor growth and spread [52]. Considering the significant amount of cell detachment that occurred following infection, we speculated that focal adhesion kinase (FAK) might be one of the primary pathways affected by ORFV (Fig. 5A). FAK is a crucial component that combines signals from growth factors and cell adhesion [74]. Autophosphorylation of FAK at Tyr-397 was found to be significant during cell adhesion. By monitoring FAK

and its phosphorylation level at Y397, we found that there was a decrease in the overall expression of FAK in all the cell lines following ORFV infection. Additionally, we observed a more significant reduction in the phosphorylation of FAK at Y397 in NPC cells than in A549 cells at 48 hpi (Fig. 5B and D). The phosphorylation of FAK at Y397 is critical for the recruitment of other SH2-containing proteins, which in turn triggers a survival signal by forming PIP2/3 phospholipids and activating AKT [75]. Therefore, we assessed AKT activation following ORFV infection. Notably, a substantial reduction in AKT phosphorylation was observed in all the cell lines after ORFV exposure (Fig. 5B and C). We suspected that the decrease in AKT phosphorylation in ORFV-infected NPC cells was a consequence of reduced FAK phosphorylation. Nonetheless, the mechanism by which ORFV modulates the FAK-AKT signaling axis warrants further investigation.

To date, numerous oncolytic viruses have been found to provoke robust immune responses against cancer [76]. However, only a few studies have reported their capacity to stimulate NK cell responses [24, 77, 78]. ORFV, which is a major regimen for cancer therapy, possesses immunomodulatory properties [79]. Syngeneic mouse models have shown that ORFV infection primarily triggers an antitumor response through the secretion of cytokines and the activation of NK cells [21]. The aim of the present study was to validate the capacity of ORFV to influence the NK cell-driven anticancer immune reaction through *in vitro* NK cell tests, which tracked the movement of NK cells and their capacity to destroy cells. This study revealed that both wild-type and VEGF-deficient recombinant viruses were able to stimulate NK cell chemotaxis by altering the extracellular environment of virus-infected NPC cells, a finding that has not been previously reported (Fig. 6C and D). On average, the VEGF-deficient mutant virus had a greater promoting effect on NK cells than the CBP-deficient mutant virus did in both NPC cell lines. Notably, synergistic tumor cytolysis, facilitated by NK cells in combination with ORFVs, was observed in both HK-1 and TW02 cells (Fig. 6A and B). The reduced tumor lysis effect observed with VEGF- and CBP-deficient ORFV strains in NK cell co-culture may be attributed to multiple factors. VEGF has immunomodulatory functions, and its deletion could impact immune cell recruitment and activation. Additionally, CBP is involved in viral replication and host immune evasion; therefore, its deletion might alter the virus-host interactions that enhance NK cell cytotoxicity. Although these deletions enhance ORFV safety, they may also attenuate certain immune-mediated effects. The results of this study align with those of two previous investigations that revealed the involvement of natural killer (NK) cells in

reducing the load of tumors through the use of oncolytic virotherapy mediated by the Orf virus (ORFV) [21, 24].

While our study primarily focused on NK cell-mediated cytotoxicity, ORFV infection likely engages additional immune components within the tumor micro-environment. Macrophages, dendritic cells, and T cells play crucial roles in shaping the immune response following viral infection [80]. ORFV has been reported to influence macrophage polarization, which may contribute to tumor clearance through pro-inflammatory cytokine release [81]. Additionally, dendritic cells could enhance antigen presentation, potentially leading to adaptive immune activation and T cell-mediated tumor suppression [81, 82]. Although our study primarily assessed NK cell involvement, these findings suggest that ORFV treatment may have a broader immunostimulatory effect. Future studies should investigate the recruitment and functional activation of additional immune cell populations, including CD8⁺T cells and tumor-associated macrophages, to fully understand the immunological impact of ORFV therapy. These considerations highlight the potential of ORFV as a multifaceted immunotherapeutic agent, capable of inducing direct tumor cell lysis while simultaneously modulating the immune micro-environment to enhance anti-tumor immunity. Expanding immune profiling in future research will be essential to validate these mechanisms and optimize ORFV-based virotherapy strategies.

Oncolytic viruses employ multiple mechanisms of action to combat cancer, including direct destruction of cancer cells, disruption of blood vessels, and stimulation of the body's immune system to fight cancer [13]. As shown in Fig. 7, the use of ORFVs (both wild-type and deletion mutants) resulted in the inhibition of HK1 tumor growth in nude mice. Moreover, H&E staining revealed a substantially greater proportion of tumor necrosis and fewer viable NPC cells in tumors that received ORFV treatment than in those in the PBS control group. (Figure 8A-H and M). Additionally, an increase in the number of tumor-infiltrating lymphocytes and neutrophils was observed in tumors that received treatment with either the wild-type ORFV or either of the two mutant ORFVs. Their presence in the tumor immune microenvironment plays a crucial role in anti-tumor immunity [83]. A significant correlation exists between an increase in tumor-infiltrating immune cells and more favorable disease outcomes as well as a greater probability of responding to immunotherapy [84]. In our xenograft mouse model, NK cells could directly attack cancer cells [85], and neutrophils could exert antitumor effects after ORFV inoculation [86]. The infiltration of these cells into the tumor site indicates an active anti-tumor immune response [87]. Hence, their presence in NPC cells after viral treatment renders ORFV, especially

our two attenuated ORFVs, an ideal candidate for establishing therapeutic regimens for NPC cells. Importantly, immunohistochemical staining and PCR confirmed the presence of the viral F1L antigen (Fig. 8I-L) and B2L gene (Fig. 8N), respectively, suggesting that tumor suppression is attributed to the productive infection of both WT and deletion mutant viruses, leading to cytolysis of tumor cells and consequently eliciting an antitumor immune response.

Conclusions

Our results suggest that ORFV could be a highly effective option for NPC, with the single gene deletion recombinant ORFVs offering a potentially safer therapeutic alternative compared to the virus with an intact genome. Among the two attenuated ORFVs, CBPΔ-EGFP was more infectious than the VEGF-defective ORFV was, especially in HK-1 cells. Moreover, ORFV likely induces cell death in NPC cells by activating unconventional GSDME-mediated pyroptosis and inhibiting FAK-AKT-transduced survival signals. These ORFV-induced cytotoxic events further triggered the cytolytic activity of NK cells against both HK-1 and TW02 cells in vitro, which was supported by the ORFV-induced regression of tumor growth in vivo. Importantly, CBPΔ and VEGFΔ null-mutant ORFVs showed selective antitumor effects that were comparable to those of WT-EGFP when tested in an animal model. A full understanding of the mechanisms underlying the oncolytic effects of ORFV will be beneficial in establishing strategies to optimize oncolytic viral therapies.

Supplementary Information

The online version contains supplementary material available at <https://doi.org/10.1186/s12985-025-02672-3>.

Supplementary Material 1

Acknowledgements

The project was supported by the National Science and Technology Council, Taiwan (111-2313-B-005-043-MY3), as well as partly by the iEGG and Animal Biotechnology Center from the Feature Areas Research Center Program within the framework of the Higher Education Sprout Project by the Ministry of Education (MOE-112-S-0023-A) in Taiwan. The funders had no role in the study design, data collection and interpretation, or decision to submit the work for publication.

Author contributions

YY, YCW, HPL and WLH conceived and designed the study. YY, YCW, and CYT verified the results. YY, CYT, HPL, SCL, GRL, and FYL performed the in vitro analyses. YY, YCW, GRG, JWJ, MLW, and YYC performed the in vivo analyses. YY, GRG, JWJ, and the three pathologists interpreted the IHC results. YY and CCC performed the formal analyses and data curation of the study. YY and WLH wrote the manuscript. WLH supervised the entire project. WLH provided funding for this study. All the authors have read and approved the manuscript.

Data availability

No datasets were generated or analysed during the current study.

Declarations

Ethical approval

All applicable international, national, and institutional guidelines for the care and use of animals were followed. The use of animals and experimental protocols were approved by the IACUC of National Chung Hsing University (approval number: 110–106).

Competing interests

The authors declare no competing interests.

Author details

¹Graduate Institute of Microbiology and Public Health, College of Veterinary Medicine, National Chung Hsing University, Taichung, Taiwan

²Graduate Institute of Veterinary Pathobiology, College of Veterinary Medicine, National Chung Hsing University, Taichung, Taiwan

³Department of Veterinary Medicine, College of Veterinary Medicine, National Chung Hsing University, Taichung, Taiwan

⁴Department of Pathology, Corazon Locsin Montelibano Memorial Regional Hospital, Bacolod City, Philippines

⁵Department Biomedical Sciences and Engineering, National Central University, Taoyuan, Taiwan

⁶Department of Microbiology and Immunology, School of Medicine, Chung Shan Medical University, Taichung, Taiwan

⁷Department of Animal Healthcare, Hungkuang University, Taichung, Taiwan

⁸The iEGG and Animal Biotechnology Center, National Chung Hsing University, Taichung, Taiwan

Received: 2 October 2024 / Accepted: 17 February 2025

Published online: 25 February 2025

References

- Jemal A, Bray F, Center MM, Ferlay J, Ward E, Forman D. Global cancer statistics. *CA Cancer J Clin*. 2011;61(2):69–90.
- Neller MA, Lopez JA, Schmidt CW. Antigens for cancer immunotherapy. *Semin Immunol*. 2008;20(5):286–95.
- Shin EJ, Wanna GB, Choi B, Aguila D 3rd, Ebert O, Genden EM, Woo SL. Interleukin-12 expression enhances vesicular stomatitis virus oncolytic therapy in murine squamous cell carcinoma. *Laryngoscope*. 2007;117(2):210–4.
- Haslam A, Kim MS, Prasad V. Updated estimates of eligibility for and response to genome-targeted oncology drugs among US cancer patients, 2006–2020. *Ann Oncol*. 2021;32(7):926–32.
- Chan WM, McFadden G. Oncolytic Poxviruses. *Annu Rev Virol*. 2014;1(1):119–41.
- Guo ZS. Oncolytic immunotherapy for metastatic cancer: lessons and future strategies. *Ann Transl Med*. 2020;8(17):1113.
- Tian Y, Xie D, Yang L. Engineering strategies to enhance oncolytic viruses in cancer immunotherapy. *Signal Transduct Target Ther*. 2022;7(1):117.
- Breitbach CJ, Paterson JM, Lemay CG, Falls TJ, McGuire A, Parato KA, et al. Targeted inflammation during oncolytic virus therapy severely compromises tumor blood flow. *Mol Ther*. 2007;15(9):1686–93.
- Lawler SE, Speranza MC, Cho CF, Chiocca EA. Oncolytic viruses in Cancer Treatment: a review. *JAMA Oncol*. 2017;3(6):841–9.
- Srinivasan Rajsri K, Rao M. Poxvirus-driven human diseases and emerging therapeutics. *Ther Adv Infect Dis*. 2022;9:20499361221136751.
- Guo ZS, Lu B, Guo Z, Giehl E, Feist M, Dai E, et al. Vaccinia virus-mediated cancer immunotherapy: cancer vaccines and oncolytics. *J Immunother Cancer*. 2019;7(1):6.
- Miller JD, van der Most RG, Akondy RS, Glidewell JT, Albott S, Masopust D, et al. Human effector and memory CD8+ T cell responses to smallpox and yellow fever vaccines. *Immunity*. 2008;28(5):710–22.
- Kirn DH, Thorne SH. Targeted and armed oncolytic poxviruses: a novel multi-mechanistic therapeutic class for cancer. *Nat Rev Cancer*. 2009;9(1):64–71.
- Wang G, Barrett JW, Stanford M, Werden SJ, Johnston JB, Gao X, et al. Infection of human cancer cells with myxoma virus requires akt activation via interaction with a viral ankyrin-repeat host range factor. *Proc Natl Acad Sci U S A*. 2006;103(12):4640–5.
- Scaltriti M, Baselga J. The epidermal growth factor receptor pathway: a model for targeted therapy. *Clin Cancer Res*. 2006;12(18):5268–72.
- Cao GD, He XB, Sun Q, Chen S, Wan K, Xu X, et al. The Oncolytic Virus in Cancer diagnosis and treatment. *Front Oncol*. 2020;10:1786.
- Moehler M, Heo J, Lee HC, Tak WY, Chao Y, Paik SW, et al. Vaccinia-based oncolytic immunotherapy Pexastimogene Devacirepvec in patients with advanced hepatocellular carcinoma after sorafenib failure: a randomized multicenter phase IIb trial (TRAVERSE). *Oncoimmunology*. 2019;8(8):1615817.
- Breitbach CJ, Bell JC, Hwang TH, Kirn DH, Burke J. The emerging therapeutic potential of the oncolytic immunotherapeutic pexa-vec (JX-594). *Oncolytic Virother*. 2015;4:25–31.
- Park SH, Breitbach CJ, Lee J, Park JO, Lim HY, Kang WK, et al. Phase 1b trial of Biweekly Intravenous Pexa-Vec (JX-594), an oncolytic and immunotherapeutic Vaccinia Virus in Colorectal Cancer. *Mol Ther*. 2015;23(9):1532–40.
- Zhou Q, Gu X, Xu Z, Huang R, Huang J, Li H, et al. [Preparation and application of anti-envelope protein B2L mouse polyclonal antibody of ORF virus]. *Xi Bao Yu Fen Zi Mian Yi Xue Za Zhi*. 2018;34(11):1036–40.
- Rintoul JL, Lemay CG, Tai LH, Stanford MM, Falls TJ, de Souza CT, et al. ORFV: a novel oncolytic and immune stimulating parapoxvirus therapeutic. *Mol Ther*. 2012;20(6):1148–57.
- Chen D, Wang R, Long M, Li W, Xiao B, Deng H, et al. Identification of in vitro and in vivo oncolytic effect in colorectal cancer cells by Orf virus strain NA1/11. *Oncol Rep*. 2021;45(2):535–46.
- Huang Y, Gong K, Chen J, Deng H, Weng K, Wu H, et al. Preclinical efficacy and involvement of mTOR signaling in the mechanism of Orf virus against nasopharyngeal carcinoma cells. *Life Sci*. 2022;291:120297.
- van Vloten JP, Matuszewska K, Minow MAA, Minott JA, Santry LA, Pereira M et al. Oncolytic Orf virus licenses NK cells via cDC1 to activate innate and adaptive antitumor mechanisms and extends survival in a murine model of late-stage ovarian cancer. *J Immunother Cancer*. 2022;10(3).
- Lin J, Sun S, Zhao K, Gao F, Wang R, Li Q, et al. Oncolytic Parapoxvirus induces Gasdermin E-mediated pyroptosis and activates antitumor immunity. *Nat Commun*. 2023;14(1):224.
- Choi AH, O’Leary MP, Chaurasiya S, Lu J, Kim SI, Fong Y, Chen NG. Novel chimeric parapoxvirus CF189 as an oncolytic immunotherapy in triple-negative breast cancer. *Surgery*. 2018;163(2):336–42.
- Baujat B, Audry H, Bourhis J, Chan AT, Onat H, Chua DT, et al. Chemotherapy in locally advanced nasopharyngeal carcinoma: an individual patient data meta-analysis of eight randomized trials and 1753 patients. *Int J Radiat Oncol Biol Phys*. 2006;64(1):47–56.
- Lin CT, Wong CI, Chan WY, Tzung KW, Ho JK, Hsu MM, Chuang SM. Establishment and characterization of two nasopharyngeal carcinoma cell lines. *Lab Invest*. 1990;62(6):713–24.
- Huang DP, Ho JH, Poon YF, Chew EC, Saw D, Lui M, et al. Establishment of a cell line (NPC/HK1) from a differentiated squamous carcinoma of the nasopharynx. *Int J Cancer*. 1980;26(2):127–32.
- Makowska A, Weiskirchen R. Nasopharyngeal carcinoma cell lines: Reliable Alternatives to primary nasopharyngeal cells? *Cells*. 2024;13(7).
- Yamada Y, Chuang ST, Tseng CY, Liao GR, Liu SW, Tseng YY, et al. Deletion of gene OV132 attenuates Orf virus more effectively than gene OV112. *Appl Microbiol Biotechnol*. 2023;107(2–3):835–51.
- Tseng YY, Lin FY, Cheng SF, Tschärke D, Chulakasian S, Chou CC, et al. Functional analysis of the short isoform of Orf virus protein OV20.0. *J Virol*. 2015;89(9):4966–79.
- Crowley LC, Scott AP, Marfell BJ, Boughaba JA, Chojnowski G, Waterhouse NJ. Measuring cell death by Propidium Iodide Uptake and Flow Cytometry. *Cold Spring Harb Protoc*. 2016;2016:7.
- Crowley LC, Marfell BJ, Scott AP, Boughaba JA, Chojnowski G, Christensen ME, Waterhouse NJ. Dead cert: measuring cell death. *Cold Spring Harb Protoc*. 2016;2016:12.
- Oldham SM, Cox AD, Reynolds ER, Sizemore NS, Coffey RJ Jr, Der CJ. Ras, but not src, transformation of RIE-1 epithelial cells is dependent on activation of the mitogen-activated protein kinase cascade. *Oncogene*. 1998;16(20):2565–73.
- Yamada Y, Liao GR, Tseng CY, Tseng YY, Hsu WL. Establishment and characterization of transformed goat primary cells by expression of simian virus 40 large T antigen for Orf virus propagations. *PLoS ONE*. 2019;14(12):e0226105.
- Kuroda S, Kubota T, Aoyama K, Kikuchi S, Tazawa H, Nishizaki M, et al. Establishment of a non-invasive semi-quantitative bioluminescent imaging method for monitoring of an Orthotopic Esophageal Cancer Mouse Model. *PLoS ONE*. 2014;9(12):e114562.
- Li Q, O’Neil M, Xie L, Caridha D, Zeng Q, Zhang J, et al. Assessment of the prophylactic activity and pharmacokinetic profile of oral tafenoquine

- compared to primaquine for inhibition of liver stage malaria infections. *Malar J*. 2014;13:141.
39. Feldman AT, Wolfe D. Tissue processing and hematoxylin and eosin staining. *Methods Mol Biol*. 2014;1180:31–43.
40. Shackelford C, Long G, Wolf J, Okerberg C, Herbert R. Qualitative and quantitative analysis of nonneoplastic lesions in toxicology studies. *Toxicol Pathol*. 2002;30(1):93–6.
41. Rziha H, Henkel M, Cottone R, Bauer B, Auge U, Gotz F, et al. Generation of recombinant parapoxviruses: non-essential genes suitable for insertion and expression of foreign genes. *J Biotechnol*. 2000;83(1–2):137–45.
42. Li W, Hao W, Peng Y, Duan C, Tong C, Song D, et al. Comparative genomic sequence analysis of Chinese orf virus strain NA1/11 with other parapoxviruses. *Arch Virol*. 2015;160(1):253–66.
43. Chi X, Zeng X, Li W, Hao W, Li M, Huang X, et al. Genome analysis of Orf virus isolates from goats in the Fujian Province of southern China. *Front Microbiol*. 2015;6:1135.
44. Chan KW, Yang CH, Lin JW, Wang HC, Lin FY, Kuo ST, et al. Phylogenetic analysis of parapoxviruses and the C-terminal heterogeneity of viral ATPase proteins. *Gene*. 2009;432(1–2):44–53.
45. Chen CC, Liu HP, Chao M, Liang Y, Tsang NM, Huang HY, et al. NF-kappaB-mediated transcriptional upregulation of TNFAIP2 by the Epstein-Barr virus oncoprotein, LMP1, promotes cell motility in nasopharyngeal carcinoma. *Oncogene*. 2014;33(28):3648–59.
46. Liu HP, Chen CC, Wu CC, Huang YC, Liu SC, Liang Y, et al. Epstein-Barr virus-encoded LMP1 interacts with FGD4 to activate Cdc42 and thereby promote migration of nasopharyngeal carcinoma cells. *PLoS Pathog*. 2012;8(5):e1002690.
47. Wang LJ, Hsu CW, Chen CC, Liang Y, Chen LC, Ojcius DM, et al. Interactome-wide analysis identifies end-binding protein 1 as a crucial component for the speck-like particle formation of activated absence in melanoma 2 (AIM2) inflammasomes. *Mol Cell Proteom*. 2012;11(11):1230–44.
48. Chung IC, Chen LC, Tsang NM, Chuang WY, Liao TC, Yuan SN, et al. Mitochondrial oxidative phosphorylation Complex regulates NLRP3 inflammasome activation and predicts patient survival in nasopharyngeal carcinoma. *Mol Cell Proteom*. 2020;19(1):142–54.
49. Chen LC, Wang LJ, Tsang NM, Ojcius DM, Chen CC, Ouyang CN, et al. Tumour inflammasome-derived IL-1beta recruits neutrophils and improves local recurrence-free survival in EBV-induced nasopharyngeal carcinoma. *EMBO Mol Med*. 2012;4(12):1276–93.
50. Yu H, Gao M, Ma Y, Wang L, Shen Y, Liu X. Inhibition of cell migration by focal adhesion kinase: time-dependent difference in integrin-induced signaling between endothelial and hepatoblastoma cells. *Int J Mol Med*. 2018;41(5):2573–88.
51. Song G, Ouyang G, Bao S. The activation of Akt/PKB signaling pathway and cell survival. *J Cell Mol Med*. 2005;9(1):59–71.
52. Boagni DA, Ravirala D, Zhang SX. Current strategies in engaging oncolytic viruses with antitumor immunity. *Mol Ther Oncolytics*. 2021;22:98–113.
53. Warricker F, Khakoo SI, Blunt MD. The role of NK cells in oncolytic viral therapy: a focus on hepatocellular carcinoma. *J Transl Genet Genom*. 2021;5:304–22.
54. Kim Y, Yoo JY, Lee TJ, Liu J, Yu J, Caligiuri MA, et al. Complex role of NK cells in regulation of oncolytic virus-bortezomib therapy. *Proc Natl Acad Sci U S A*. 2018;115(19):4927–32.
55. Xu Y, Zhou S, Lam YW, Pang SW. Dynamics of Natural Killer cells cytotoxicity in Microwell arrays with connecting channels. *Front Immunol*. 2017;8:998.
56. Zhao JJ, Pan K, Li JJ, Chen YB, Chen JG, Lv L, et al. Identification of LZAP as a new candidate tumor suppressor in hepatocellular carcinoma. *PLoS ONE*. 2011;6(10):e26608.
57. Chiocci EA. Oncolytic viruses. *Nat Rev Cancer*. 2002;2(12):938–50.
58. Deng H, Xiao B, Huang Y, Weng K, Chen J, Li K, et al. The combined use of Orf Virus and PAK4 inhibitor exerts anti-tumor effect in breast Cancer. *Front Microbiol*. 2022;13:845259.
59. Rziha HJ, Rohde J, Amann R. Generation and Selection of Orf Virus (ORFV) Recombinants. *Methods Mol Biol*. 2016;1349:177–200.
60. Coradduzza E, Sanna D, Scarpa F, Azzena I, Fiori MS, Scivoli R et al. A deeper insight into evolutionary patterns and phylogenetic history of ORF virus through the whole genome sequencing of the first Italian strains. *Viruses*. 2022;14(7).
61. Seet BT, McCaughan CA, Handel TM, Mercer A, Brunetti C, McFadden G, Fleming SB. Analysis of an orf virus chemokine-binding protein: shifting ligand specificities among a family of poxvirus viroceptors. *Proc Natl Acad Sci U S A*. 2003;100(25):15137–42.
62. Lyttle DJ, Fraser KM, Fleming SB, Mercer AA, Robinson AJ. Homologs of vascular endothelial growth factor are encoded by the poxvirus orf virus. *J Virol*. 1994;68(1):84–92.
63. van Sluijs L, Pijlman GP, Kammenga JE. Why do individuals differ in viral susceptibility? A story told by Model organisms. *Viruses*. 2017;9(10).
64. Park JH, Gail MH, Weinberg CR, Carroll RJ, Chung CC, Wang ZM, et al. Distribution of allele frequencies and effect sizes and their interrelationships for common genetic susceptibility variants. *P Natl Acad Sci USA*. 2011;108(44):18026–31.
65. Li YI, van de Geijn B, Raj A, Knowles DA, Petti AA, Golan D, et al. RNA splicing is a primary link between genetic variation and disease. *Science*. 2016;352(6285):600–4.
66. Gasch AP, Payseur BA, Pool JE. The power of natural variation for Model Organism Biology. *Trends Genet*. 2016;32(3):147–54.
67. Palanivelu L, Liu CH, Lin LT. Immunogenic cell death: the cornerstone of oncolytic viro-immunotherapy. *Front Immunol*. 2022;13:1038226.
68. Prestwich RJ, Harrington KJ, Pandha HS, Vile RG, Melcher AA, Errington F. Oncolytic viruses: a novel form of immunotherapy. *Expert Rev Anticancer Ther*. 2008;8(10):1581–8.
69. Lee S, Hirohama M, Noguchi M, Nagata K, Kawaguchi A. Influenza A virus infection triggers pyroptosis and apoptosis of respiratory epithelial cells through the type I Interferon Signaling Pathway in a mutually exclusive manner. *J Virol*. 2018;92(14).
70. Rogers C, Fernandes-Alnemri T, Mayes L, Alnemri D, Cingolani G, Alnemri ES. Cleavage of DFNA5 by caspase-3 during apoptosis mediates progression to secondary necrotic/pyroptotic cell death. *Nat Commun*. 2017;8:14128.
71. Guo ZS, Liu Z, Bartlett DL. Oncolytic immunotherapy: dying the right way is a key to eliciting Potent Antitumor Immunity. *Front Oncol*. 2014;4:74.
72. Bommareddy PK, Zloza A, Rabkin SD, Kaufman HL. Oncolytic virus immunotherapy induces immunogenic cell death and overcomes STING deficiency in melanoma. *Oncoimmunology*. 2019;8(7):1591875.
73. Fucikova J, Kepp O, Kasikova L, Petroni G, Yamazaki T, Liu P, et al. Detection of immunogenic cell death and its relevance for cancer therapy. *Cell Death Dis*. 2020;11(11):1013.
74. Bauer MS, Baumann F, Daday C, Redondo P, Durner E, Jobst MA, et al. Structural and mechanistic insights into mechanoactivation of focal adhesion kinase. *Proc Natl Acad Sci U S A*. 2019;116(14):6766–74.
75. Roy-Luzarraga M, Hodivala-Dilke K. Molecular pathways: endothelial cell FAK-A target for Cancer Treatment. *Clin Cancer Res*. 2016;22(15):3718–24.
76. Melcher A, Parato K, Rooney CM, Bell JC. Thunder and lightning: immunotherapy and oncolytic viruses collide. *Mol Ther*. 2011;19(6):1008–16.
77. Prestwich RJ, Ilett EJ, Errington F, Diaz RM, Steele LP, Kottke T, et al. Immune-mediated antitumor activity of reovirus is required for therapy and is independent of direct viral oncolysis and replication. *Clin Cancer Res*. 2009;15(13):4374–81.
78. Boudreau JE, Stephenson KB, Wang F, Ashkar AA, Mossman KL, Lenz LL, et al. IL-15 and type I interferon are required for activation of tumoricidal NK cells by virus-infected dendritic cells. *Cancer Res*. 2011;71(7):2497–506.
79. Bakar AM, Jesse FFA, Abdullah CAC, Noordin MM, Lawan Z, Mangga HK et al. Immunomodulatory strategies for Parapoxvirus: current status and future approaches for the development of vaccines against Orf Virus infection. *Vaccines (Basel)*. 2021;9(11).
80. von Buttler H, Siegemund S, Buttner M, Alber G. Identification of toll-like receptor 9 as Parapoxvirus ovis-sensing receptor in plasmacytoid dendritic cells. *PLoS ONE*. 2014;9(8):e106188.
81. Minott JA, van Vloten JP, Yates JGE, Santry LA, Matuszewska K, Pereira M, et al. Kinetic analysis of oncolytic OrfV-induced innate and adaptive immune responses in a murine model of late-stage ovarian cancer. *Mol Ther Oncolytics*. 2023;31:100748.
82. Feng Q, Li L, Du G, Liu Y, Liu X, Wu J, Shang Y. Proteomic analyses reveal that Orf virus induces the activation and maturation of mouse bone marrow-derived dendritic cells. *Res Vet Sci*. 2020;132:563–73.
83. Whiteside TL, Heo DS, Takagi S, Herberman RB. Tumor-infiltrating lymphocytes from human solid tumors: antigen-specific killer T lymphocytes of activated natural killer lymphocytes. *Immunol Ser*. 1989;48:139–57.
84. Melsesen MM, Sheybani ND, Leick KM, Slingluff CL, Jr. Barriers to immune cell infiltration in tumors. *J Immunother Cancer*. 2023;11(4).
85. Ye K, Li F, Wang R, Cen T, Liu S, Zhao Z, et al. An armed oncolytic virus enhances the efficacy of tumor-infiltrating lymphocyte therapy by converting tumors to artificial antigen-presenting cells in situ. *Mol Ther*. 2022;30(12):3658–76.

86. Pylaeva E, Korschunow G, Spyra I, Bordbari S, Siakaeva E, Ozel I, et al. During early stages of cancer, neutrophils initiate anti-tumor immune responses in tumor-draining lymph nodes. *Cell Rep.* 2022;40(7):111171.
87. Furumaya C, Martinez-Sanz P, Bouti P, Kujipers TW, Matlung HL. Plasticity in Pro- and anti-tumor activity of neutrophils: shifting the balance. *Front Immunol.* 2020;11:2100.

Publisher's note

Springer Nature remains neutral with regard to jurisdictional claims in published maps and institutional affiliations.